Neuropharmacology 65 (2013) 74–82

Contents lists available at SciVerse ScienceDirect

Neuropharmacology

journal homepage: www.elsevier.com/locate/neuropharm

Methamphetamine-induced nitric oxide promotes vesicular transport in blood–brain barrier endothelial cells

Tânia Martins [a,b,c], Thomas Burgoyne [a], Bridget-Ann Kenny [a], Natalie Hudson [a], Clare E. Futter [a], António F. Ambrósio [c,d], Ana P. Silva [b,c], John Greenwood [a], Patric Turowski [a,*]

[a] Cell Biology, UCL Institute of Ophthalmology, 11-43 Bath Street, London EC1V 9EL, UK
[b] Laboratory of Pharmacology and Experimental Therapeutics, Faculty of Medicine, University of Coimbra, 3004-548 Coimbra, Portugal
[c] Institute of Biomedical Research on Light and Image (IBILI), Faculty of Medicine, University of Coimbra, 3004-548 Coimbra, Portugal
[d] Centre of Ophthalmology and Vision Sciences, IBILI, Faculty of Medicine, University of Coimbra, 3004-548 Coimbra, Portugal

ARTICLE INFO

Article history:
Received 29 March 2012
Received in revised form
15 August 2012
Accepted 21 August 2012

Keywords:
Methamphetamine
Fluid-phase transcytosis
Blood–brain barrier
Transendothelial leukocyte migration
Nitric oxide

ABSTRACT

Methamphetamine's (METH) neurotoxicity is thought to be in part due to its ability to induce blood–brain barrier (BBB) dysfunction. Here, we investigated the effect of METH on barrier properties of cultured rat primary brain microvascular endothelial cells (BMVECs). Transendothelial flux doubled in response to METH, irrespective of the size of tracer used. At the same time, transendothelial electrical resistance was unchanged as was the ultrastructural appearance of inter-endothelial junctions and the distribution of key junction proteins, suggesting that METH promoted vesicular but not junctional transport. Indeed, METH significantly increased uptake of horseradish peroxidase into vesicular structures. METH also enhanced transendothelial migration of lymphocytes indicating that the endothelial barrier against both molecules and cells was compromised. Barrier breakdown was only observed in response to METH at low micromolar concentrations, with enhanced vesicular uptake peaking at 1 μM METH. The BMVEC response to METH also involved rapid activation of endothelial nitric oxide synthase and its inhibition abrogated METH-induced permeability and lymphocyte migration, indicating that nitric oxide was a key mediator of BBB disruption in response to METH. This study underlines the key role of nitric oxide in BBB function and describes a novel mechanism of drug-induced fluid-phase transcytosis at the BBB.

1. Introduction

The BBB regulates the exchange of nutrients, waste and immune cells between the blood and the nervous tissue of the central nervous system (CNS) and is the most important component preserving CNS homeostasis and neuronal function (Abbott et al., 2010). Barrier function is epitomised by the restriction of ionic currents across the BBB, with electrical resistance reaching 1500–2000 Ω cm^2 in vivo (Crone and Olesen, 1982; Butt et al., 1990). The barrier-conferring cellular equivalent of the BBB are the endothelial cells (ECs) of the brain capillary network. However associated pericytes, astrocytes and the basement membrane also play an additional regulatory and structural role. Many BBB mechanisms can be modelled in vitro using monocultures of brain microvascular endothelial cells (BMVECs) (Perriere et al., 2007; Roux and Couraud, 2005). Importantly, such BMVEC models retain the features that render the BBB such a formidable barrier, namely a full complement of tight junctions (TJs), lack of fenestrations and low fluid-phase endocytosis (pinocytosis) (Abbott et al., 2010). At the healthy BBB, molecule transport in and out of the CNS is carried out by carrier-mediated transport systems or receptor- and adsorptive-mediated transcytosis. In certain- mostly pathological-conditions, molecules can also cross the BBB endothelium non-specifically via a paracellular pathway. Indeed, BBB dysfunction involving transient or even chronic opening of TJs contributes to the pathogenesis of many diverse CNS pathologies, such as epilepsy, Parkinson's and Alzheimer's disease, and multiple sclerosis (Forster, 2008; Zlokovic, 2008). More anecdotally, enhanced fluid-phase endocytosis or (macro)pinocytosis has been reported in BBB ECs in response to hypoxic or ischemic conditions (Kaur and Ling, 2008), indicating that this is a transport feature which is rarely used by either the healthy or diseased BBB.

Methamphetamine (METH) is a highly addictive psychostimulant with neurotoxic features. Like other amphetamines and presumably because of its similarity to dopamine, METH causes monoamine release at neuronal synapses, primarily through the

* Corresponding author. Tel.: +44 207 608 6970; fax: +44 207 608 6810.
E-mail address: p.turowski@ucl.ac.uk (P. Turowski).

0028-3908
http://dx.doi.org/10.1016/j.neuropharm.2012.08.021

inhibition of plasmalemmal transporters such as the dopamine transporter or the serotonin transporter (Cruickshank and Dyer, 2009). It also causes long-term damage to monoaminergic nerve terminals, as well as excitotoxicity, mitochondrial dysfunction and increased production of reactive oxygen and nitrogen species (ROS and RNS, respectively) (Quinton and Yamamoto, 2006). Because of its small size and lipophilicity, METH readily crosses the BBB by non-specific diffusion. In addition, METH can induce BBB dysfunction in rodents (Kiyatkin et al., 2007; Sharma and Ali, 2006), in particular in the limbic region (Bowyer and Ali, 2006) including the hippocampus (Martins et al., 2011). It is now assumed that, in addition to direct damage of monoaminergic nerve terminals, the deregulation of the BBB in these brain areas potentially contributes to widespread METH-induced neurotoxicity.

Nitric oxide synthases (NOS) convert L-arginine to produce the second messenger nitric oxide (NO). Two NOS isoforms exist in ECs: endothelial NOS (eNOS), which is expressed constitutively, and inducible NOS (iNOS), which is synthesised and utilized during long-term adaptation of the vasculature (Michel and Feron, 1997). In vascular ECs, eNOS regulates many key functions including angiogenesis, inflammatory and anti-inflammatory processes, and is the main NOS system regulating barrier function and permeability (Fukumura et al., 2001; Schubert et al., 2002). The activity of eNOS is primarily regulated by reversible phosphorylation in response to various stimuli including vascular endothelial growth factor (VEGF), insulin or shear stress, and phosphorylation on S1177 is considered to be a reliable indicator of its activation status (Fleming, 2010). The activation and activity of eNOS is also intimately linked to that of caveolin-1 and caveolae and thus fluid-phase endocytosis (Simionescu et al., 2009).

The purpose of the present study was to investigate the effect of METH in a system of primary BMVECs with very well-preserved TJs and barrier function. BMVEC permeability and the underlying mechanism were evaluated in response to METH exposure. Since pathophysiological BBB breakdown is often associated with enhanced leukocyte infiltration, alterations to lymphocyte migration were also studied. METH effects were assessed at concentrations, which are physiologically significant, i.e. at levels found in drug abusers. Finally, since NO production may play an important role in METH-induced monoaminergic neurotoxicity (Imam et al., 2000), we tested the role of eNOS in the METH-induced EC response.

2. Materials and methods

2.1. Materials

Unless otherwise stated all materials were from Sigma. METH was provided by Drs Nuno Milhazes (Institute of Health Sciences-North, Gandra PRD, Portugal) and Fernanda Borges (Faculty of Sciences, University of Oporto, Portugal).

2.2. Brain microvascular endothelial cells (BMVECs)

Microvessels were isolated from brains of 6–8 week-old female Lewis rats (Abbott et al., 1992) and seeded onto collagen IV/fibronectin-coated tissue culture ware or 12-mm Costar Transwells (3460) at high density (vessels from 6 rat brains per 40 cm^2). Cells were grown in EGM2-MV (Lonza, Wokingham, United Kingdom) [with 5 μg/ml puromycin during the first 5 days (Perriere et al., 2007)] for 2–3 weeks until their transendothelial electric resistance (TEER) plateaued at values above 200 Ω cm^2. The immortalized Lewis rat cell line GPNT, which maintains many of the signalling and metabolic features of primary BMVECs (but not TJs and well-developed barrier properties) (Martinelli et al., 2009; Roux and Couraud, 2005) was maintained in Ham's F10 supplemented with 10% foetal calf serum, 2 ng/ml bFGF, 80 μg/ml heparin, 100 U/ml penicillin and 100 μg/ml streptomycin.

2.3. Transendothelial flux

Fluorescein (FITC) or rhodamine B isothiocyanate (RITC)-dextran of 4, 70 or 250 kDa was added at 1 mg/ml to the apical side of BMVEC grown on 12-mm Transwell filters. Samples (50 μl) were removed from the basal chamber (and replaced by fresh medium) at 20–30 min intervals for 120 min before and after addition of METH and/or L-NG-Nitroarginine methyl ester (L-NAME). Fluorescence of samples was measured in a FLUOstar OPTIMA microplate reader (BMG LABTECH, Aylesbury, UK), plotted against time and permeability changes were determined from linear slope changes before and after addition of compounds.

2.4. Transendothelial electrical resistance (TEER)

TEER of primary brain EC monolayers was measured using STX-2 chopstick electrodes connected to an EVOM epithelial voltohmmeter (World Precision Instruments, Herts, UK). Real time TEER changes during METH treatment were monitored by impedance spectroscopy using a 1600R ECIS system (Applied Biophysics, Troy, NY, USA). For this, ECs were seeded on collagen type IV/fibronectin-coated 8W10E electrode arrays (Applied Biophysics). Impedance was measured at 4000 Hz at 10-min intervals. After the cells reached stable impedance, the ECs were either left untreated or treated with 1 or 50 μM METH. Results were normalised and averaged from at least 3 independent experiments.

2.5. Immunocytochemistry

Confluent BMVECs were fixed in 80% methanol, 3.2% formaldehyde, 0.05 M HEPES, pH 7.4 (−20 °C) for 5 min and then processed for indirect immunocytochemistry (Turowski et al., 2004). Primary antibodies included affinity purified anti-vascular endothelial cadherin (VEC) (see supplemental Material and Methods for more details), and anti-claudin-5 (1:100), occludin (1:50) and zonula occludens (ZO)-1 (1:50) (Zymed Lab, San Francisco, CA, USA). Immunostained preparations were mounted using Moviol 4-88 and analysed on a confocal laser-scanning microscopy LSM 700 system (Carl Zeiss, Hertfordshire, UK). Series of overlapping 0.35 μm sections spanning the entire cell thickness were recorded.

2.6. Horseradish peroxidase uptake and transport

For transport studies, horseradish peroxidase (HRP, 10 mg/ml) was added with or without 1 μM METH to the apical side of confluent primary BMVECs grown on 12-mm Costar Transwells filters. After 1 h cells were washed 3 times with warm HBSS containing Ca^{2+} and Mg^{2+} and new medium was added. Samples (100 μl) were removed from the basal chamber (and replaced by fresh medium) at 30-min intervals for 120 min. Samples were reacted with 100 μl of 1 mg/ml o-phenylenediamine and 1 μl/ml of 30% hydrogen peroxide and, after colour appearance, stopped with 100 μl of 1 N HCl. Absorbance of each sample was measured in a FLUOstar OPTIMA microplate reader (BMG LABTECH, Aylesbury, UK). HRP activity was plotted against time and rates determined by linear regression.

Uptake studies were performed in a similar fashion. Primary BMVECs grown in 96-well plates were treated with METH at various concentrations and for up to 70 min as specified in the Figure Legends. Subsequently, HRP (1 mg/ml) was added for 5–30 min (optimal times were determined as shown in Suppl. Fig. S3). Cells were then extensively washed with warm HBSS and lysed with 50 μl of 1% Triton X-100 in PBS before adding o-phenylenediamine and hydrogen peroxide.

2.7. Electron microscopy

Primary ECs were grown to confluence on collagen type IV/fibronectin-coated polycarbonate filters. Cells were either directly processed for fixation or, for the visualisation of vesicular uptake, HRP (10 mg/ml) was added to the apical side of cells, and cells either left untreated or treated with METH (1 μM). Where indicated, ECs were preincubated with L-NAME (1 mM, 1 h) before HRP and METH addition. After 1 h of incubation, monolayers were washed with DPBS and then fixed in 2% paraformaldehyde, 2% glutaraldehyde, in 0.05 M cacodylate buffer for 30 min. For the diaminobenzide (DAB) reaction, cells were incubated with 3% DAB, 30% hydrogen peroxide and imidazole in the dark for 30 min at RT. Cells were then incubated with 1.5% potassium ferricyanide, 1% Osmium tetroxide for 1 h in the dark at 4 °C, followed by a dehydration step, and finally embedded in Epon resin. The specimens were sectioned at 70 nm with no post-staining and visualised on a JEOL 1010 transmission electron microscope. The area and number of HRP-containing structures from METH treated-cells were normalised to the control values from non-treated cells, and represented as average per 1000 μm^2 of cytoplasm.

2.8. Western blotting

Primary or GPNT ECs were grown on collagen I-coated 35-mm dishes, and, at confluence, cultured in serum-free medium overnight. Cells were treated as detailed in the figure legends and then processed for western blot analysis as described previously (Martinelli et al., 2009).

2.9. Transendothelial lymphocyte migration

Primary or GPNT BMVECs were grown to confluence in collagen I-coated 96-well plates, and treated as indicated in figure legends. Cells were washed extensively and then, 2×10^5/myelin basic protein (MBP)-specific rat lymphocytes were

added and allowed to migrate for 1–4 h. After the incubation, the migration and adhesion rates were determined by time-lapse video microscopy as described (Adamson et al., 1999). Migration data was collected from multiple experiments, each representing a minimum of six wells.

2.10. Statistical analyses

Statistics were performed using one-way ANOVA, followed by Dunnett's or Bonferroni's post-test, or Student's *t*-test, as indicated in the Figure Legends. Data are presented as mean ± SEM, and the level of $P < 0.05$ was accepted as statistically significant.

3. Results

3.1. METH induces macromolecular flux across brain microvascular EC monolayers without affecting TEER

To investigate cellular and molecular mechanisms underlying METH-induced changes of the BBB we studied the response of BMVECs to METH in vitro. Unless stated otherwise, freshly prepared primary rat BMVEC (Perriere et al., 2007) were used. These cells retained many characteristics of the intact BBB such as the expression of continuous adherens and tight junctions (see Suppl. Fig. S2), low permeability to macromolecules ($0.113 \pm 0.016 \times 10^{-3}$ cm/min for 4 kDa FITC-dextran, $n = 11$), and high transendothelial electrical resistance (TEER = 345 ± 30 Ω cm^2). To exclude preparations with compromised junctional integrity, only BMVEC monolayers with TEERs plateauing at least at 200 Ω cm^2 were used in this study. The blood concentrations of METH in drug abusers are in the low micromolar range, with a medium concentration of 1.25 μM (Melega et al., 2007). Macromolecular flux of fluorescent dextrans across primary BMVEC monolayers was measured in the absence or presence of 1 μM METH. Treatment with METH resulted in a 2.07 ± 0.31 fold increase of 4 kDa FITC-dextran flux (Fig. 1A). Significantly, this increase remained unchanged even when the flux of considerable larger tracers was assessed (Fig. 1B and C). The effect of METH on endothelial electrical barrier properties was also measured by impedance spectroscopy. Impedance (and consequently the TEER) of primary rat BMVEC monolayers was not altered by the exposure to 1 μM METH (Fig. 1D), whereas lysophosphatidic acid produced a strong and transient opening of the ionic barrier (Fig. 1D). Taken together, this strongly indicated that junctional transport, which is size-selective and also involves concomitant changes in TEER (Steed et al., 2010), was not affected by exposure to METH.

3.2. Endothelial junction organisation in response to METH treatment

We examined the effect of METH on the organisation of the major junction proteins in BMVEC by immunocytochemistry followed by confocal microscopy. In unstimulated cells, staining of VE-cadherin (VEC), occludin and zonula occludens-1 (ZO-1) was restricted to areas of cell–cell interaction and surrounded the entirety of each cell in uninterrupted fashion (Suppl. Fig. S2 A). Claudin-5 immunostaining was very similar but could also be detected on apical membranes and internal vesicles. High magnification confocal microscopy showed that treatment with 1 μM METH for 2 or 6 h did not disrupt the junctional continuity of VEC, occludin, claudin-5 or ZO-1 staining (Fig. 2A). Furthermore, ultrastructural analysis of inter-endothelial junction areas of BMVEC by transmission electron microscopy (EM) revealed no discernible changes following treatment with METH (Fig. 2B). Clearly, METH did not affect the continuity of adherens or tight junctions. However, in some cells it induced additional staining for VEC and occludin in parajunctional areas (Suppl. Fig. S2 A and B). At least in the case of VEC, diffuse parajunctional staining is thought to represent junctional flow (Kametani and Takeichi, 2007), suggesting that METH did not induce global changes to inter-endothelial

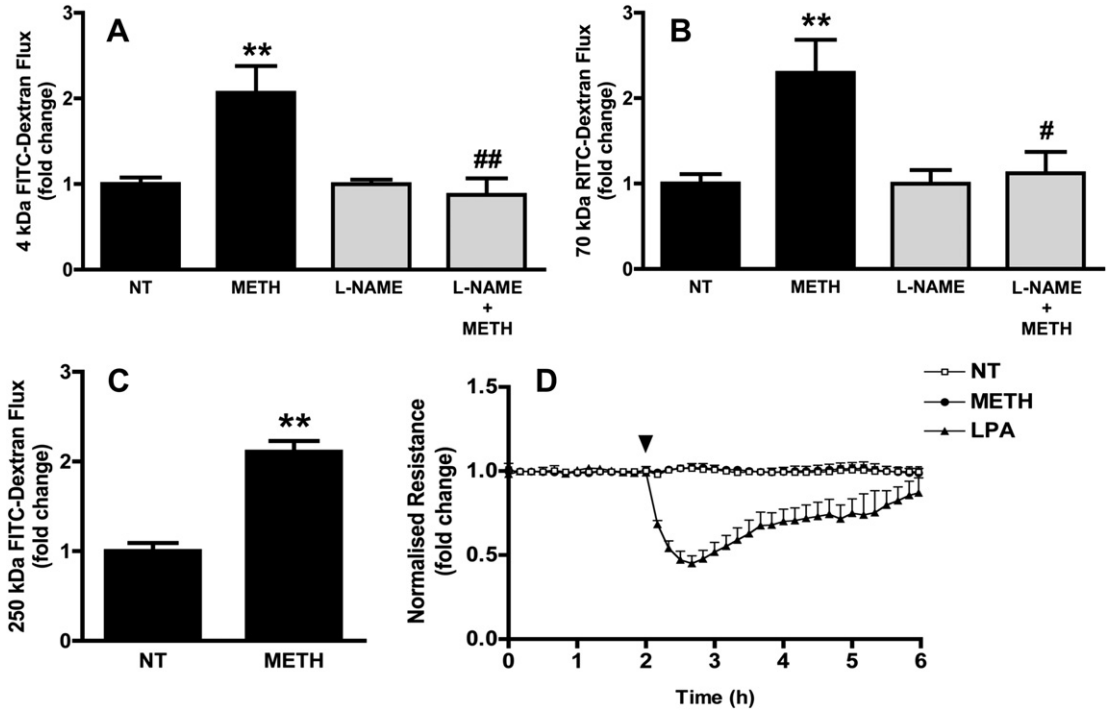

Fig. 1. METH-induced barrier breakdown in primary BMVECs. (A–C) Macromolecular flux across primary BMVEC was assessed using 4 kDa FITC dextran (A), 70 kDa RITC dextran (B) or 250 kDa FITC dextran (C). Flux was determined before and after the addition of METH (1 μM). Where indicated the cells were pre-treated with L-NAME (1 mM, 1 h) (grey bars). (D) TEER of confluent BMVECs monolayers, grown on gold electrodes, was measured by impedance spectroscopy before and after the addition (arrowhead) of 1 μM METH or 10 μM lysophosphatidic acid (LPA). All results shown are means ± SEM of at least three independent experiments. Note that only positive SEM are shown. $^{**}P < 0.01$ (Dunnett's post test vs NT); $^{\#}P < 0.05$, $^{\#\#}P < 0.01$ (Bonferroni's post test vs METH).

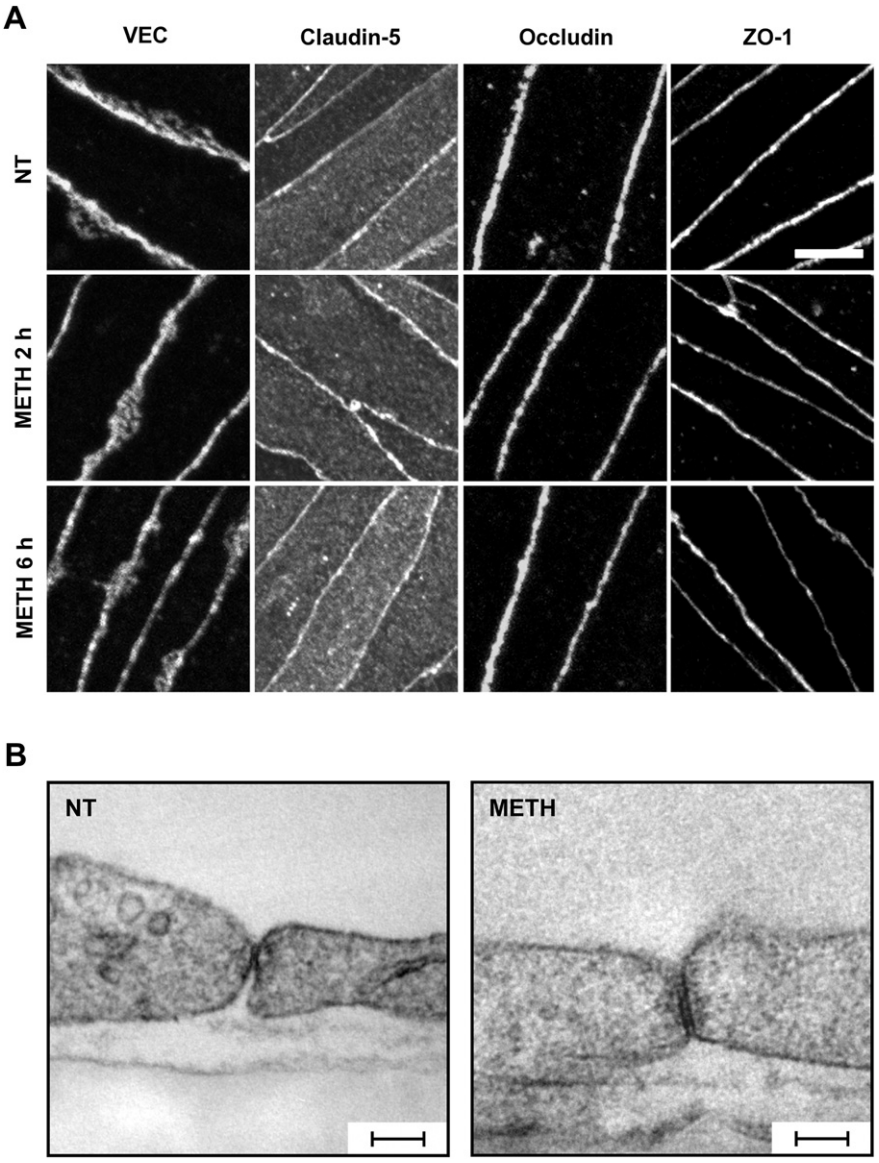

Fig. 2. Effect of METH on the organisation of the interendothelial junctions. (A) ECs were either left untreated (NT) or treated with METH (1 μM) for 2 or 6 h. Subsequently, cells were fixed and stained for VEC, claudin-5, occludin and ZO-1, and then analysed by confocal microscopy. Representative projections of overlapping 0.35 μm sections spanning the entire cell thickness showed that METH exposure did not disrupt the continuity of any junction staining. Scale bar = 5 μm. (B) ECs were either left untreated (NT) or treated with METH (1 μM) for 1 h and then analysed by transmission EM. Shown are representative images of endothelial contact areas, which appeared unchanged following METH treatment. Space bars = 100 nm.

junctions but enhanced the flow/turnover of certain junctional proteins. Importantly, METH-induced paracellular VEC and occludin staining occurred even when the junctional strands were intact (Suppl. Fig. S2 C).

3.3. METH promotes endocytosis in BMVECs

Since METH-induced permeability in ECs was not paracellular, we investigated whether the increased macromolecular flux was due to transcytosis. To test this, unidirectional, non-junctional HRP flux was measured. For this, BMVEC were allowed to take up apically presented HRP for 1 h in the absence or presence of METH. Then all extracellular HRP was washed off before comparing basal HRP efflux rates. As shown in Fig. 3A, HRP efflux was increased 1.77 ± 0.11-fold in BMVEC treated with 1 μM METH, which was a similar increase as seen for METH-induced continuous apical-to-basal dextran flux. HRP-treated cells were further analysed by EM. DAB staining revealed the presence of HRP-containing vesicular structures in all cells (Fig. 3B). HRP was detected in large structures with a diameter of at least 150 nm (morphologically resembling lysosomes), and much smaller vesicles. METH treatment did not affect HRP uptake into the large vesicular structures (data not shown) but significantly increased HRP in small vesicles [Fig. 3B(b)]. In fact, the area of such DAB staining increased nearly 1.5-fold (Fig. 3C). This was at least in part due to a significantly higher number of DAB-positive vesicles (Fig. 3D). Collectively, these data demonstrated that METH induced permeability in BMVECs was mediated by fluid-phase transcytosis.

Further analysis of HRP transport indicated that METH enhanced luminal uptake into BMVEC (Suppl. Fig. S3 and Fig. 4). HRP uptake steadily increased with METH treatment time, reaching a peak at around 55 min of METH (Fig. 4A). Under these conditions, enhanced uptake was almost exclusively restricted to METH stimulation at concentrations of 1 μM, with neither lower nor higher

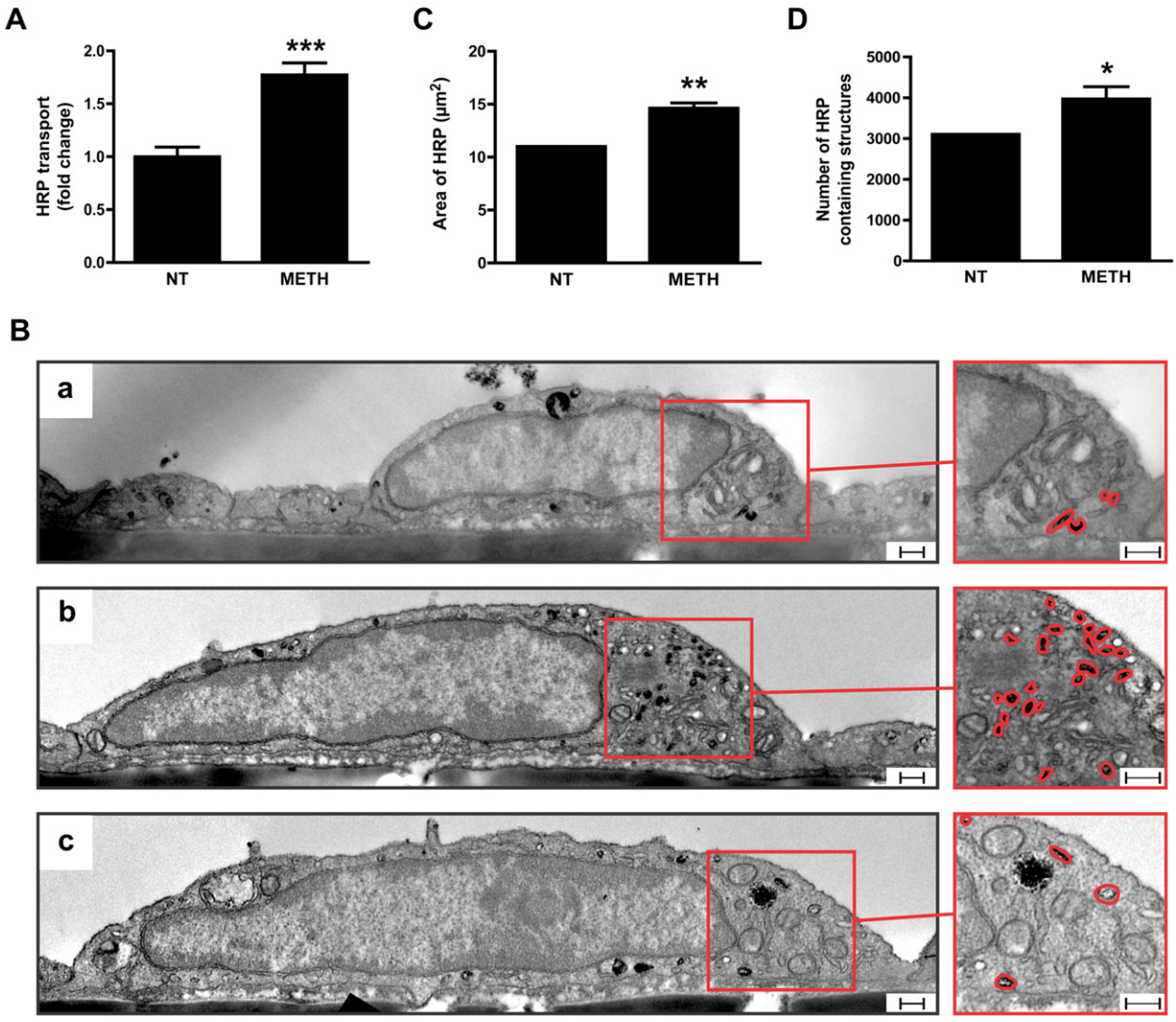

Fig. 3. METH enhances transcytosis in BMVECs. (A) Primary rat BMVECs were either left untreated (NT) or treated with METH (1 μM) for 1 h in the presence of horseradish peroxidase (HRP) on the apical side of cells. HRP was then removed and the rate of its transport to the basal side determined and compared. (B–D) Uptake of HRP by primary BMVECs visualised using transmission EM. Cells were either left untreated [B(a)] or treated with METH (1 μM) [B(b and c)] and incubated with HRP in the apical media for 1 h before fixing and processing for HRP visualisation (using DAB) and transmission EM. Shown are representative images in which electron dense DAB reaction products revealed the presence of HRP-containing compartments. [B(c)] Additional pre-treatment with L-NAME (1 mM, 1 h) prevented METH-induced accumulation of HRP-containing structures. Scale bar = 250 nm. Densitometric quantification of the area (C) of DAB staining or (D) number of DAB-positive vesicles per 1000 μm^2 of cytoplasm, showing a significant increase with METH treatment. The results are expressed as mean ± SEM of at least three independent experiments. $^*P < 0.05$, $^{**}P < 0.01$, $^{***}P < 0.001$ (Student's *t*-test), significant when compared to NT.

doses significantly affecting HRP uptake (Fig. 4B), indicating that the dose used throughout this study produced maximal effects.

3.4. Enhanced lymphocyte transendothelial migration (TEM) following METH treatment

The BBB not only forms a formidable regulated barrier to blood borne molecules but also to immune and cancer cells (Greenwood et al., 2011; Weil et al., 2005). We analysed the effect of METH on lymphocyte TEM across primary BMVEC monolayers. Pre-treatment with 1 μM METH for 30 min or 2 h resulted in a significant increase in the migration rate of T-cells across primary ECs (Fig. 5A). Similarly, exposure of immortalised GPNT ECs to 1 μM METH also enhanced TEM of T-cells (Fig. 5B). This suggested that METH induced dysfunction of the endothelial barrier against cells and molecules alike.

3.5. eNOS mediates METH-induced effects in BMVECs

Transcytosis in ECs occurs mainly via caveolae (Predescu et al., 2007). Since eNOS activation is functionally linked to caveolae (Maniatis et al., 2006), endothelial permeability (Fukumura et al., 2001; Schubert et al., 2002) and lymphocyte TEM (Martinelli et al., 2009), we investigated whether it was involved in the BMVEC response to METH. Activation of eNOS was determined by measuring phosphorylation on S1177. Exposure of primary BMVECs to 1 μM METH induced eNOS S1177 phosphorylation (Fig. 6A). Levels of eNOS phosphorylation increased significantly within 30 min of METH exposure, plateaued after 1 h, and persisted for at least 2 h. We observed a similar response to METH in the GPNT BMVEC cell line, indicating that the biochemical response to METH was preserved even after EC immortalisation (Fig. 6B). We next investigated whether eNOS inhibition attenuated any of the barrier-disrupting effects of METH. Pre-treatment of primary

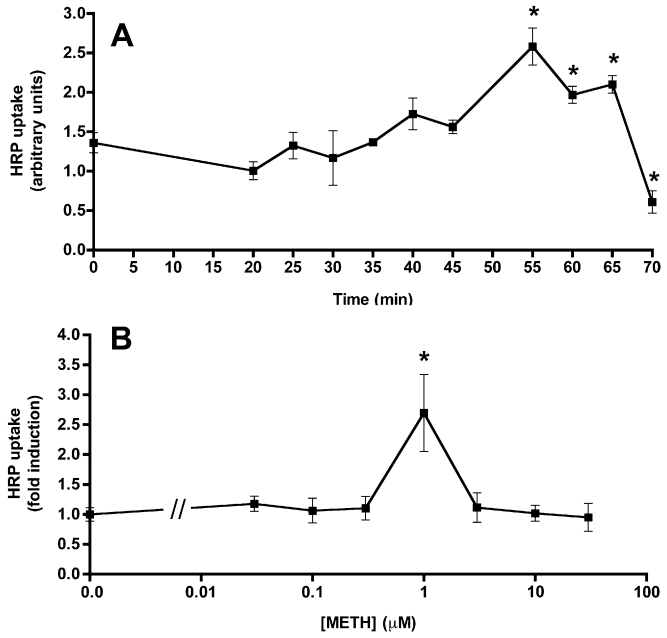

Fig. 4. METH enhances HRP uptake in time- and concentration-responsive manner. (A) Primary BMVECs were treated with METH (1 μM) for the indicated times followed by HRP (1 mg/ml) addition. After 5 min, extracellular HRP was washed off, before cell lysis and HRP quantification. Shown are mean levels of intracellular HRP ± SEM ($n = 3$). $^{*}P < 0.05$ (Student's t-test), significant when compared to time 0. (B) Primary BMVECs were treated with METH at the indicated concentrations for 55 min. Subsequently, HRP (1 mg/ml) was added for 5 min. Cells were extensively washed and intracellular HRP was determined in cell lysates. Shown are mean levels of intracellular HRP ± SEM ($n = 10$). $^{*}P < 0.05$ (Student's t-test), significant when compared to no METH treatment.

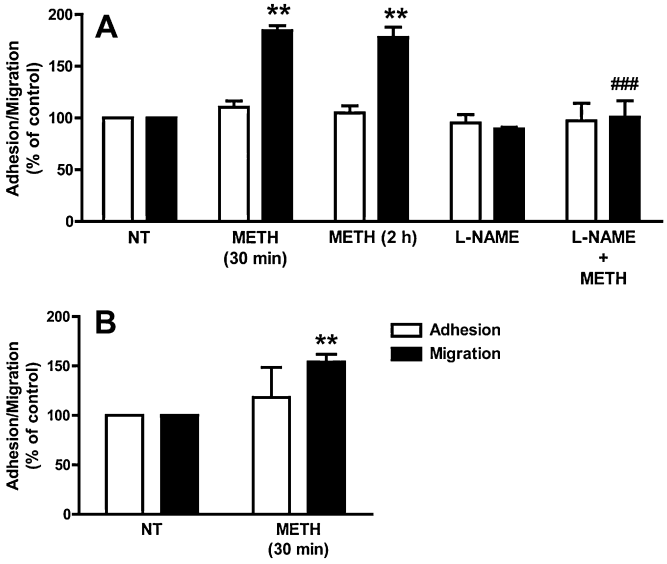

Fig. 5. METH enhances transendothelial lymphocyte migration. (A) Primary BMVECs were either left untreated (NT) or treated with METH (1 μM) for the indicated times. Cells were then washed before MBP-specific rat lymphocytes were added and allowed to adhere and migrate for 4 h (A). Shown are adhesion (white bars) and migration rates (black bars) as % of control cells (NT) (mean ± SEM of six replicates from at least three independent experiments) ($^{**}P < 0.01$, Dunnett's post test). Pre-incubation with L-NAME (1 mM, 1 h) prevented the increase in migration induced by 30-min METH ($^{###}P < 0.001$, Bonferroni's post test vs METH 30 min). (B) As in A, except that lymphocytes were allowed to adhere and migrate across GPNT ECs for 1 h ($^{**}P < 0.01$, Student's t-test).

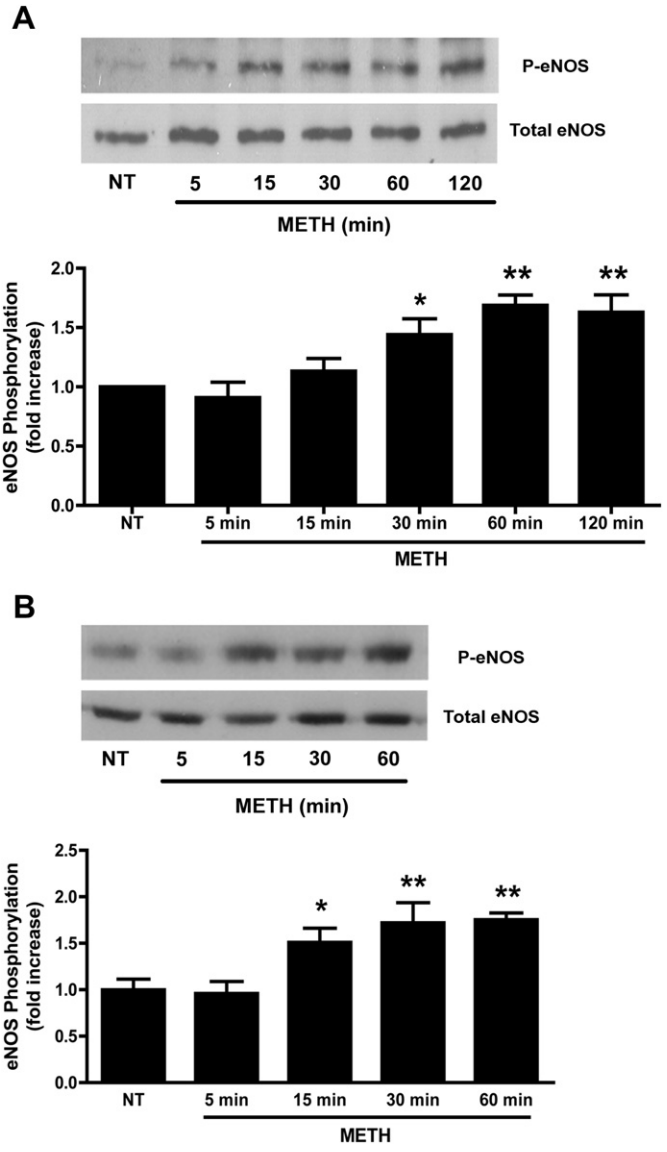

Fig. 6. METH activates eNOS in BMVECs. (A) Primary BMVECs were either left untreated (NT) or treated with METH (1 μM) for the indicated times. Total protein extracts (ca. 50 μg) were analysed by immunoblotting with anti-phospho-S1177 eNOS antibodies. The blot was subsequently stripped and probed for total eNOS. (B) As in A, except that GPNT BMVECs were used. Densitometric quantification (normalised means ± SEM) of three independent experiments is shown on the bottom of each panel. $^{*}P < 0.05$, $^{**}P < 0.01$ (Dunnett's post test vs NT).

BMVEC with L-NAME entirely inhibited the METH-induced increase of macromolecular flux (Fig. 1A and B, grey columns). Moreover, L-NAME also prevented the accumulation of HRP-positive vesicles in response to METH [Fig. 3B(c)]. Finally, pre-treatment of primary BMVEC with L-NAME also prevented enhanced lymphocyte TEM in response to METH (Fig. 5A). Taken together, these data indicated that eNOS activation and NO production was central to METH-induced barrier impairment.

3.6. Absence of effects following exposure to higher METH concentrations

Since HRP uptake studies indicated that METH was only effective at doses around 1 μM (Fig. 4), we tested whether higher METH concentrations affected any of the other parameters reported in this study. Importantly, the treatment with METH at concentrations

of up to 100 μM for up to 24 h did not affect EC viability (Suppl. Fig. S4). GPNT ECs were exposed to METH at concentrations varying between 1 and 100 μM, and 1 h later, eNOS activation was measured. In agreement with our HRP uptake studies, only exposure to METH at 1 μM led to significant eNOS activation (Fig. 7A). Furthermore, when permeability changes across primary BMVECs were assessed in response to 50 μM METH, we found no effect on macromolecular flux (Fig. 7B and C) or TEER (Fig. 7D). Lastly, a higher concentration of METH (50 μM) did not affect lymphocytes TEM either (Fig. 7E). Collectively, these data suggested that, in our BBB in vitro models, METH led to maximal barrier disruption at concentrations of 1 μM as judged by effects on eNOS activity, EC permeability, vesicular uptake and lymphocyte TEM.

4. Discussion

METH directly damages dopaminergic and serotonergic nerve terminals but also induces BBB dysfunction, which is thought to contribute to its neurotoxicity (Silva et al., 2010). It is conceivable that BBB dysfunction is an indirect result of pathophysiological changes following METH administration, such as hyperthermia (Kiyatkin et al., 2007). In the present study and in agreement with published work (Ramirez et al., 2009), we demonstrate that METH acts directly on cultured primary BMVEC to compromise their barrier properties. In addition, we provide mechanistic evidence that barrier breakdown was due to eNOS activation and enhanced transcytosis.

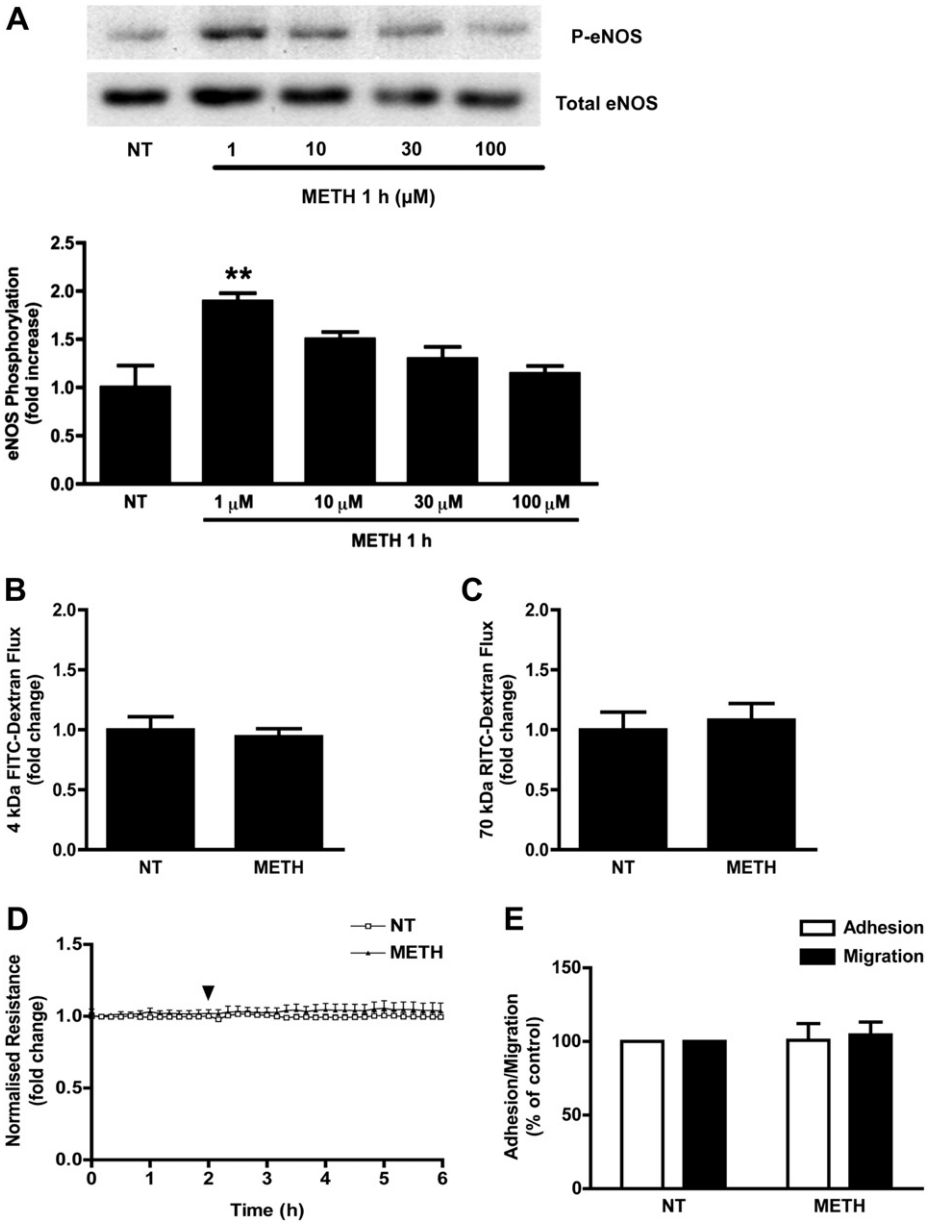

Fig. 7. Effect of higher METH concentrations in BMVECs. (A) GPNT ECs were either left untreated (NT) or treated with METH during 1 h with the indicated METH concentrations. eNOS phosphorylation was quantified by immunoblotting as described in Fig. 5. (**$P < 0.01$, Dunnett's post test). (B, C) Changes in flux of 4 kDa FITC-dextran (B) or 70 kDa RITC-dextran (C) across primary BMVECs in response to 50 μM METH was measured as described in Fig. 1. (D) TEER changes were measured in monolayers of primary BMVECs in response to 50 μM METH as described in Fig. 1. (E) GPNT ECs were either left untreated or treated with METH (50 μM, 30 min) before lymphocyte adhesion (white) and migration (black) was determined as described in Fig. 5.

For our study, we have used primary rat BMVEC as a system of high reproducibility and statistical robustness. We introduced modifications to standard isolation procedures, namely selection with puromycin (Perriere et al., 2007) and direct seeding at high density (extensive growth periods of BMVEC lead to loss of TJ proteins), to generate monocultures of high purity and unmatched barrier properties as assessed by TJ protein expression and TEER. Exposure of these cells to METH did not affect interendothelial junction integrity. Despite mild changes to the staining pattern of VEC and occludin, which suggested altered protein turnover, the lateral continuity of all assessed junction proteins remained unchanged following METH exposure. In agreement, changes in TEER, considered a robust readout for junction opening (Steed et al., 2010), were not observed in response to METH. Small changes in the level of TJ proteins are seen in the METH-treated mouse brain (Martins et al., 2011). However, it is unclear whether these changes occur in BBB ECs and whether they result in reduced junction integrity. Rather than enhanced paracellular permeability, we found clear evidence for enhanced transcytosis in response to METH. Dextrans of varying size and HRP were transported at equally enhanced rate, suggesting that fluid-phase transcytosis was operational (Hawkins and Egleton, 2008). Furthermore, METH induced time and concentration-dependent vesicular uptake of HRP. In agreement with a transcellular transport pathway, EM revealed numerous plasma membrane invaginations reminiscent of caveolae but not HRP-positive clathrin-coated vesicles (Suppl. Fig. S5). This is in line with the notion that caveolae are the principal vesicular structure for transcytosis in ECs (Predescu et al., 2007; Simionescu et al., 2009). Significantly, METH also induces fluid-phase endocytosis in cultured neurons (Nara et al., 2010), suggesting that this response may not be restricted to ECs. Non-specific fluid-phase transcytosis is rarely observed in the healthy BBB endothelium (Abbott et al., 2010) but has been associated with hypertension, hypoxia and ischemia although effector mechanisms are unknown (Cipolla et al., 2004; Kaur and Ling, 2008). Here we provide first evidence that fluid-phase transcytosis across BMVEC can be directly enhanced by a small molecule, namely METH.

BBB dysfunction often results in increased leukocyte TEM. Exposure to METH enhanced lymphocyte TEM, in agreement with reports using a low barrier BMVEC line and monocytes (Park et al., 2012; Ramirez et al., 2009). Leukocyte TEM utilises both paracellular and transcellular pathways (Muller, 2011). Since the effective dose of METH left endothelial junctions intact and increased vesicular transport in primary BMVECs, it appears likely that transcellular TEM was enhanced. Vesiculo-vacuolar organelles (VVOs), which form channels for the passage of macromolecules and are responsible for enhanced permeability in the tumour vasculature, were initially suggested as possible endothelial structures that could mediate transcellular migration (Hordijk, 2006). Subsequently, Muller and co-workers showed that the lateral border recycling compartment (LBRC), a membrane reticulum involved in membrane and junction protein trafficking in cell border areas of ECs, is implicated in regulating both transcellular and paracellular TEM (Muller, 2011). As judged by transmission EM, METH typically induced HRP uptake into large groups of juxtapositional vesicular structures, which were restricted to a single area of the cell (as illustrated in Fig. 3). Since images were derived from 70 nm thick sections it was impossible to determine whether HRP was taken up into isolated vesicles or a reticulum similar or identical to the LBRC. Thus, METH may influence membrane availability and/or dynamics of the LBRC or the VVOs and thus diminish barrier properties to molecules and cells in BMVECs.

Both METH-enhanced transcytosis and TEM were sensitive to pre-treatment with the NOS inhibitor L-NAME. Since effective doses of METH also led to robust eNOS activation and iNOS could not be detected at any time during our experiments (data not shown), we conclude that eNOS activation and consequent NO production are key factors of METH-induced BBB breakdown. Activation of neuronal NOS and the production of NO and derivatives also occur in METH-stimulated neurons and have been implicated in associated dopaminergic neurotoxicity (Imam et al., 2000), suggesting again that cellular METH targets may be similar in neurons and ECs. In the endothelium, eNOS is instrumental in regulating vascular permeability (Fukumura et al., 2001; Schubert et al., 2002). Activation of eNOS and NO production are also limiting factors of lymphocyte TEM across BMVEC (Martinelli et al., 2009). Thus, by activating eNOS, METH clearly modulated a central regulator of BMVEC barrier function. Most cytotoxicity associated with NO is due to peroxynitrite, the reaction product between NO and the superoxide anion (Pacher et al., 2007). Our study did not address whether barrier breakdown was merely due to NO or rather peroxynitrite. However, acute microvascular permeability and lymphocyte TEM are mainly dependent on NO but not superoxide production (Duran et al., 2010; Martinelli et al., 2009). Furthermore, we were unable to detect any cytotoxicity in BMVEC in response to METH, suggesting that oxidative stress and peroxynitrite production was not induced.

Typical METH abuse leads to accumulation of the drug in blood plasma at sub or low micromolar concentrations (Cook et al., 1992; Harris et al., 2003; Melega et al., 2007). In primary rat BMVEC, HRP uptake and eNOS activation were only observed in response to METH at ca. 1 μM. In agreement, endothelial barrier dysfunction was observed at low but not high micromolar concentrations of METH, suggesting that the BBB is compromised under typical abuse conditions. This raises the possibility that several targets with different affinities for METH exist in ECs. Alternatively, higher concentrations of METH may induce rapid down-regulation of the EC response and render it undetectable. Finally, higher METH concentration may also lead to the activation of another signalling pathway counteracting the primary response described in this report. Indeed, higher concentrations of METH lead to the generation of ROS (Fleckenstein et al., 2007; Park et al., 2012; Ramirez et al., 2009), which may subsequently neutralise the bioavailable NO. Nevertheless, it is unclear whether research into the BMVEC response to higher METH concentration is justified since concentrations of METH higher than 30 μM are associated with lethality in humans (Takayasu et al., 1995).

In summary, our results suggest that METH-induced opening of the BBB involves eNOS/NO-mediated transcytosis. Apart from providing important mechanistic insight into METH-induced neurotoxicity, our work also identifies a potentially novel strategy for drug delivery into the brain. METH has been suggested for such use before (Kast, 2009), but our finding of a link to non-specific fluid-phase transcytosis, which is usually absent at the BBB, increases the significance of potential use for this purpose. To fully assess the possibility of agonist-induced opening of the BBB, future work should focus on identifying the endothelial targets of METH and the structural determinants of METH that are important for BMVEC deregulation. Potentially, this could lead to the design of non-psychostimulatory METH derivatives that maintain the capacity to transiently open the BBB without associated toxicity to monoaminergic nerve terminals.

Acknowledgements

We thank Drs Nuno Milhazes (Institute of Health Sciences-North, Gandra PRD, Portugal) and Fernanda Borges (Faculty of Sciences, University of Oporto, Portugal) for providing the methamphetamine used in this study. This work was supported by Foundation for Science and Technology (FCT) Grants PTDC/SAU-

FCF/67053/2006 and PTDC/SAU-FCF/098685/2008 (COMPETE and FEDER funds), and Fellowship SFRH/BD/41019/2007 from FCT co-financed by QREN (European Social Fund), the Wellcome Trust and the British Heart Foundation.

Appendix A. Supplementary data

Supplementary data related to this article can be found at http://dx.doi.org/10.1016/j.neuropharm.2012.08.021.

References

Abbott, N.J., Hughes, C.C., Revest, P.A., Greenwood, J., 1992. Development and characterisation of a rat brain capillary endothelial culture: towards an in vitro blood–brain barrier. J. Cell. Sci. 103 (Pt 1), 23–37.

Abbott, N.J., Patabendige, A.A., Dolman, D.E., Yusof, S.R., Begley, D.J., 2010. Structure and function of the blood–brain barrier. Neurobiol. Dis. 37, 13–25.

Adamson, P., Etienne, S., Couraud, P.O., Calder, V., Greenwood, J., 1999. Lymphocyte migration through brain endothelial cell monolayers involves signaling through endothelial ICAM-1 via a rho-dependent pathway. J. Immunol. 162, 2964–2973.

Bowyer, J.F., Ali, S., 2006. High doses of methamphetamine that cause disruption of the blood–brain barrier in limbic regions produce extensive neuronal degeneration in mouse hippocampus. Synapse 60, 521–532.

Butt, A.M., Jones, H.C., Abbott, N.J., 1990. Electrical resistance across the blood–brain barrier in anaesthetized rats: a developmental study. J. Physiol. 429, 47–62.

Cipolla, M.J., Crete, R., Vitullo, L., Rix, R.D., 2004. Transcellular transport as a mechanism of blood–brain barrier disruption during stroke. Front. Biosci. 9, 777–785.

Cook, C.E., Jeffcoat, A.R., Sadler, B.M., Hill, J.M., Voyksner, R.D., Pugh, D.E., White, W.R., Perez-Reyes, M., 1992. Pharmacokinetics of oral methamphetamine and effects of repeated daily dosing in humans. Drug Metab. Dispos. 20, 856–862.

Crone, C., Olesen, S.P., 1982. Electrical resistance of brain microvascular endothelium. Brain Res. 241, 49–55.

Cruickshank, C.C., Dyer, K.R., 2009. A review of the clinical pharmacology of methamphetamine. Addiction 104, 1085–1099.

Duran, W.N., Breslin, J.W., Sanchez, F.A., 2010. The NO cascade, eNOS location, and microvascular permeability. Cardiovasc. Res. 87, 254–261.

Fleckenstein, A.E., Volz, T.J., Riddle, E.L., Gibb, J.W., Hanson, G.R., 2007. New insights into the mechanism of action of amphetamines. Annu. Rev. Pharmacol. Toxicol. 47, 681–698.

Fleming, I., 2010. Molecular mechanisms underlying the activation of eNOS. Pflugers Arch. 459, 793–806.

Forster, C., 2008. Tight junctions and the modulation of barrier function in disease. Histochem. Cell. Biol. 130, 55–70.

Fukumura, D., Gohongi, T., Kadambi, A., Izumi, Y., Ang, J., Yun, C.O., Buerk, D.G., Huang, P.L., Jain, R.K., 2001. Predominant role of endothelial nitric oxide synthase in vascular endothelial growth factor-induced angiogenesis and vascular permeability. Proc. Natl. Acad. Sci. U. S. A. 98, 2604–2609.

Greenwood, J., Heasman, S.J., Alvarez, J.I., Prat, A., Lyck, R., Engelhardt, B., 2011. Review: leucocyte–endothelial cell crosstalk at the blood–brain barrier: a prerequisite for successful immune cell entry to the brain. Neuropathol. Appl. Neurobiol. 37, 24–39.

Harris, D.S., Boxenbaum, H., Everhart, E.T., Sequeira, G., Mendelson, J.E., Jones, R.T., 2003. The bioavailability of intranasal and smoked methamphetamine. Clin. Pharmacol. Ther. 74, 475–486.

Hawkins, B.T., Egleton, R.D., 2008. Pathophysiology of the blood–brain barrier: animal models and methods. Curr. Top. Dev. Biol. 80, 277–309.

Hordijk, P.L., 2006. Endothelial signalling events during leukocyte transmigration. FEBS J. 273, 4408–4415.

Imam, S.Z., Islam, F., Itzhak, Y., Slikker Jr., W., Ali, S.F., 2000. Prevention of dopaminergic neurotoxicity by targeting nitric oxide and peroxynitrite: implications for the prevention of methamphetamine-induced neurotoxic damage. Ann. N. Y. Acad. Sci. 914, 157–171.

Kametani, Y., Takeichi, M., 2007. Basal-to-apical cadherin flow at cell junctions. Nat. Cell. Biol. 9, 92–98.

Kast, R.E., 2009. Use of FDA approved methamphetamine to allow adjunctive use of methylnaltrexone to mediate core anti-growth factor signaling effects in glioblastoma. J. Neurooncol. 94, 163–167.

Kaur, C., Ling, E.A., 2008. Blood brain barrier in hypoxic-ischemic conditions. Curr. Neurovasc. Res. 5, 71–81.

Kiyatkin, E.A., Brown, P.L., Sharma, H.S., 2007. Brain edema and breakdown of the blood–brain barrier during methamphetamine intoxication: critical role of brain hyperthermia. Eur. J. Neurosci. 26, 1242–1253.

Maniatis, N.A., Brovkovych, V., Allen, S.E., John, T.A., Shajahan, A.N., Tiruppathi, C., Vogel, S.M., Skidgel, R.A., Malik, A.B., Minshall, R.D., 2006. Novel mechanism of endothelial nitric oxide synthase activation mediated by caveolae internalization in endothelial cells. Circ. Res. 99, 870–877.

Martinelli, R., Gegg, M., Longbottom, R., Adamson, P., Turowski, P., Greenwood, J., 2009. ICAM-1-mediated endothelial nitric oxide synthase activation via calcium and AMP-activated protein kinase is required for transendothelial lymphocyte migration. Mol. Biol. Cell. 20, 995–1005.

Martins, T., Baptista, S., Goncalves, J., Leal, E., Milhazes, N., Borges, F., Ribeiro, C.F., Quintela, O., Lendoiro, E., Lopez-Rivadulla, M., Ambrosio, A.F., Silva, A.P., 2011. Methamphetamine transiently increases the blood–brain barrier permeability in the hippocampus: role of tight junction proteins and matrix metalloproteinase-9. Brain Res. 1411, 28–40.

Melega, W.P., Cho, A.K., Harvey, D., Lacan, G., 2007. Methamphetamine blood concentrations in human abusers: application to pharmacokinetic modeling. Synapse 61, 216–220.

Michel, T., Feron, O., 1997. Nitric oxide synthases: which, where, how, and why? J. Clin. Invest. 100, 2146–2152.

Muller, W.A., 2011. Mechanisms of leukocyte transendothelial migration. Annu. Rev. Pathol. 6, 323–344.

Nara, A., Aki, T., Funakoshi, T., Uemura, K., 2010. Methamphetamine induces macropinocytosis in differentiated SH-SY5Y human neuroblastoma cells. Brain Res. 1352, 1–10.

Pacher, P., Beckman, J.S., Liaudet, L., 2007. Nitric oxide and peroxynitrite in health and disease. Physiol. Rev. 87, 315–424.

Park, M., Hennig, B., Toborek, M., 2012. Methamphetamine alters occludin expression via NADPH oxidase-induced oxidative insult and intact caveolae. J. Cell. Mol. Med. 16, 362–375.

Perriere, N., Yousif, S., Cazaubon, S., Chaverot, N., Bourasset, F., Cisternino, S., Decleves, X., Hori, S., Terasaki, T., Deli, M., Scherrmann, J.M., Temsamani, J., Roux, F., Couraud, P.O., 2007. A functional in vitro model of rat blood–brain barrier for molecular analysis of efflux transporters. Brain Res. 1150, 1–13.

Predescu, S.A., Predescu, D.N., Malik, A.B., 2007. Molecular determinants of endothelial transcytosis and their role in endothelial permeability. Am. J. Physiol. Lung Cell. Mol. Physiol. 293, L823–L842.

Quinton, M.S., Yamamoto, B.K., 2006. Causes and consequences of methamphetamine and MDMA toxicity. AAPS J. 8, E337–E347.

Ramirez, S.H., Potula, R., Fan, S., Eidem, T., Papugani, A., Reichenbach, N., Dykstra, H., Weksler, B.B., Romero, I.A., Couraud, P.O., Persidsky, Y., 2009. Methamphetamine disrupts blood–brain barrier function by induction of oxidative stress in brain endothelial cells. J. Cereb. Blood Flow Metab. 29, 1933–1945.

Roux, F., Couraud, P.O., 2005. Rat brain endothelial cell lines for the study of blood–brain barrier permeability and transport functions. Cell. Mol. Neurobiol. 25, 41–58.

Schubert, W., Frank, P.G., Woodman, S.E., Hyogo, H., Cohen, D.E., Chow, C.W., Lisanti, M.P., 2002. Microvascular hyperpermeability in caveolin-1 (−/−) knockout mice. Treatment with a specific nitric-oxide synthase inhibitor, L-NAME, restores normal microvascular permeability in Cav-1 null mice. J. Biol. Chem. 277, 40091–40098.

Sharma, H.S., Ali, S.F., 2006. Alterations in blood-brain barrier function by morphine and methamphetamine. Ann. N. Y. Acad. Sci. 1074, 198–224.

Silva, A.P., Martins, T., Baptista, S., Goncalves, J., Agasse, F., Malva, J.O., 2010. Brain injury associated with widely abused amphetamines: neuroinflammation, neurogenesis and blood–brain barrier. Curr. Drug Abuse Rev. 3, 239–254.

Simionescu, M., Popov, D., Sima, A., 2009. Endothelial transcytosis in health and disease. Cell. Tissue Res. 335, 27–40.

Steed, E., Balda, M.S., Matter, K., 2010. Dynamics and functions of tight junctions. Trends Cell. Biol. 20, 142–149.

Takayasu, T., Ohshima, T., Nishigami, J., Kondo, T., Nagano, T., 1995. Screening and determination of methamphetamine and amphetamine in the blood, urine and stomach contents in emergency medical care and autopsy cases. J. Clin. Forensic Med. 2, 25–33.

Turowski, P., Adamson, P., Sathia, J., Zhang, J.J., Moss, S.E., Aylward, G.W., Hayes, M.J., Kanuga, N., Greenwood, J., 2004. Basement membrane-dependent modification of phenotype and gene expression in human retinal pigment epithelial ARPE-19 cells. Invest. Ophthalmol. Vis. Sci. 45, 2786–2794.

Weil, R.J., Palmieri, D.C., Bronder, J.L., Stark, A.M., Steeg, P.S., 2005. Breast cancer metastasis to the central nervous system. Am. J. Pathol. 167, 913–920.

Zlokovic, B.V., 2008. The blood–brain barrier in health and chronic neurodegenerative disorders. Neuron 57, 178–201.